Simultaneous effect of mechanical alloying and arc-melting processes in the microstructure and hardness of an AlCoFeMoNiTi high-entropy alloy

F.J. Baldenebro-López, J.M. Herrera-Ramírez, S.P. Arredondo-Rea, C.D. Gómez-Esparza, **R. Martínez-Sánchez**

Abstract

A nanostructured AlCoFeMoNiTi high entropy alloy was synthesized through the mechanical alloying process. Bulk samples were obtained by two different routes to compare the microstructural evolution and hardness behavior: sintering and arc melting. Through electron microscopy analyses the formation of Mo-rich and Ti-rich phases were identified in the melted sample, while Ti-rich nano-precipitates were observed in the sintered sample. A higher microhardness value was achieved on the sintered sample than for the melted sample. The disadvantage of porosity in the sintered sample in comparison to the melted one was overcome by the hardening effect produced by the mechanical alloying.

1. Introduction

The concept of high entropy alloys (HEAs) is basically defined as alloys containing multi-principal elements in equiatomic or near equiatomic percentage [1], breaking with the conventional one or two major elements alloying approach. Since their development in the past decade, great attention has been paid to HEAs in the materials research field due to their high strength and hardness, excellent softening resistance, wear and corrosion resistance [2]; [3]; [4] ; [5], as well as by their singularity to form phases with simple structures (FCC and/or BCC).

It has been experimentally determined that each alloying element with its own

crystalline structure, atomic radio and melting point has a direct effect on the physical and chemical properties of the alloy. Most of the studied high entropy alloys contains high temperature elements like Ni, Co and Fe. The Al (FCC), although it is an element with a low melting point, low hardness and high ductility, it favors the hardening of the HEAs because is a BCC-type phase former [1]. It is important to emphasize that the simultaneous effect of Ti and Mo in high entropy alloys have been slightly reported [6] ; [7].

Powder metallurgy is a method that has been used to produce ferrous and non ferrous alloys from elemental mixtures or alloyed powders, often followed by compaction and sintering to obtain solid products. Among the techniques used to produce metal powder alloys with enhanced mechanical properties is mechanical alloying.

The high entropy alloys have been fabricated by different routes. The melting process has been the preferred technique to produce these alloys. It is well known that samples produced by mechanical alloying (MA) followed by consolidation, possess a higher pore density than samples fabricated by casting. However, the melting route leads to the segregation problem, while by the MA process, homogenous chemical distribution and solid solubility extension can be reached. In addition, the mechanical alloying is a powerful process in solid state capable to easily obtain nanocrystalline materials with superior properties. However, in the field of HEAs, the synthesis of new alloys deals with the limitations of traditional metallurgy techniques. Kunce et al. reported the synthesis of TiZrNbMoV high entropy alloys by Laser Engineered Net Shaping (LENS) from a mixture of pure

elemental powders [8]. With the aim to explore alternative routes to synthesize high entropy alloys and improve their performance, in this work the simultaneous effect of mechanical alloying and arc melting on the fabrication of an AlCoFeMoNiTi alloy was studied.

2. Experimental

Elemental powders supplied by Alfa Aesar with purity higher than 99.5% in weight (metal basis) of Al (particle size of 20 μm), Co (particle size of 25 μm), Fe (particle size of 75 μm), Mo (particle size of 5 μm), Ni (particle size of 20 μm) and Ti (particle size of 35 μm) were initially weighed and mechanically alloyed for 10 h and 20 h to obtain an equiatomic high entropy alloy. The milling was performed in a high-energy ball mill (SPEX 8000 M) under an argon atmosphere using hardened steel vial and grinding media. The ball-to-powder weight ratio was 5:1. Methanol was added as a process control agent to inhibit the particle agglomeration. The milled powders for 10 h were mechanically pressed into cylindrical samples with 5 mm of diameter under 1.5 GPa of pressure, using an uniaxial compaction die in a hydraulic press. Bulk samples were obtained by two different routes. For the first route the green specimens were sintered at 1423 K in vacuum during 3 h. For the second route the green compacts were prepared using arc melting method, were melted in a water-cooled copper mold under an argon (Ar) atmosphere to prevent oxidation after purging with argon three times. The ingots were remelted at least 5 times to improve chemical homogeneity.

The morphological and microstructural features were characterized by scanning electron microscopy (SEM, JEOL JSM-7401F) and phase composition was

identified by transmission electron microscopy (TEM, JEOL-JEM2200FS). The structural evolution was examined by X-ray diffraction (XRD) analysis in a Panalytical X'Pert PRO diffractometer with Cu Kα radiation (λ = 0.15406 nm). The hardness of the milled powders and consolidated specimens were measured by the Vickers microhardness method on the cross-section polished samples using a 50 and 200 g load, respectively.

3. Results and discussion

3.1. Powders characterization

It has been experimentally determined that the HEAs usually have structures with FCC and/or BCC phases if an appropriate combination of elements and quantities are present in such alloys. Pure elemental characteristic peaks are observed in the unmilled sample (Fig. 1). After 10 h of milling the intensity of the elemental diffraction peaks decreased and their width increased, while the corresponding peaks to BCC-type phases began to appear. A transformation of the elemental powder mixture to solid solutions occurred and the elemental pure peaks almost vanished, except the Mo and Fe peaks that slightly shifted to lower angles. The peaks presented in the AlCoFeMoNiTi mechanically alloyed (MA'ed) powders sample were identified as two BCC phases, a Mo-type (a_{BCC1} = 0.314 nm) and a Fe-type (a_{BCC2} = 0.287 nm). Their lattice parameters are very similar to those of the pure elements (a_{Mo} = 0.315 nm and a_{Fe} = 0.287 nm). The crystallite size of the present BCC phases has been determined in the range of 15.4 and 11.6 nm for powders milled during 10 and 20 h, respectively. Regarding to the lattice strain, values of 0.76% and 0.99% for powders milled during 10 and 20 h, respectively, have been

calculated. The crystal size of the as-milled powders was estimated from broadening of XRD peaks using the Scherrer equation. As milling

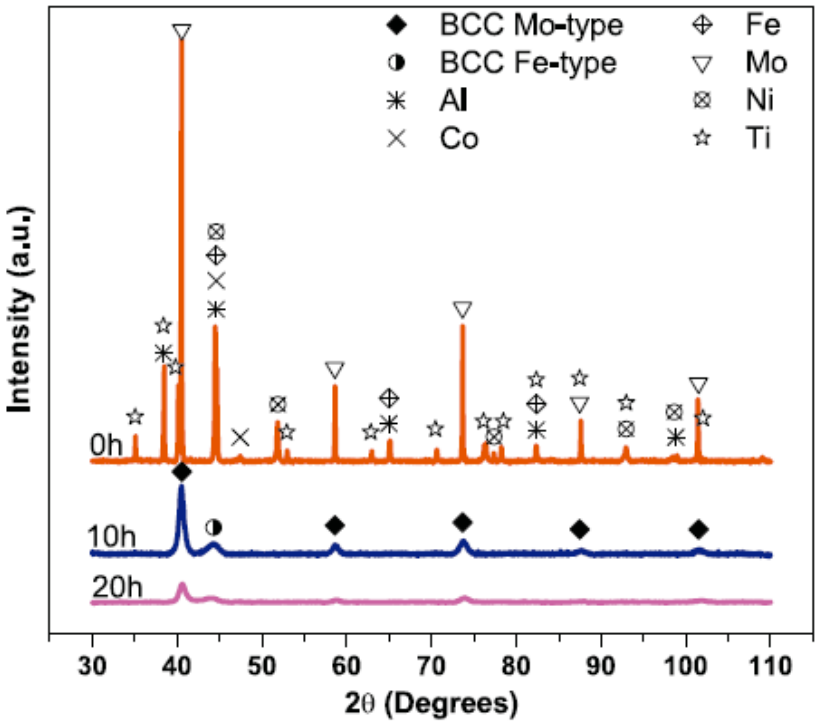

Fig. 1. XRD pattern of AlCoFeMoNiTi powders alloy after different mechanical alloying times.

continued to 20 h no further changes of phases were observed on the XRD patterns, and the powders milled for 10 h were selected to obtain bulk samples.

The mechanical alloying (MA) is a powder processing technique that enables the production of chemically and structurally homogeneous materials, starting from mixtures of elemental powders. During mechanical alloying the powder particles are trapped between the grinding media and undergo deformation and/or fracture process, and final chemical homogeneity depends upon the mechanical behavior of the starting powder components. In the literature, the EDS analyses have been widely used to determined chemical composition. In order to evaluate the possible

chemical composition variations of mechanically alloyed powders from nominal composition after milling, EDS/SEM analyses were performed and the results are presented in Table 1. It can be observed that all elements present deviations from the nominal composition, therefore it is important to take into consideration that besides possible loss of material by mechanical friction during milling, the EDS microanalysis provides only semi-quantitative results, which could present relative errors of ± 3% [9]. The variations of all elements after 10 h of milling are less than 3%.

Milling process has a significant effect over the size and morphology of particles. The intrinsic mechanical characteristics of the powders as well as their volumetric fractions affect the surface characteristics after milling. Fig. 2 shows SEM micrographs of the elemental powder mixture and milled AlCoFeMoNiTi powders after 10 h of milling. On the unmilled powders, the existence of different element particles is clearly seen. Fig. 2a shows the morphology and particle size of the starting powders: aluminum (round-shaped), cobalt (round-shaped), iron (flake-shaped), molybdenum (round-shaped), nickel (round-shaped) and titanium (flake-shaped). In the other hand, Fig. 2b displays homogeneous morphology of MA'ed powders. The continuous effect of deformation and cold welding during MA leaded to the formation of uniform particle in size, 10 h of mechanical alloying allowed the formation of particles with an average particle size of about 10 μm. At the same time, the chemical composition of individual MA'ed powders is similar to the proportion of the starting elemental powders, which was corroborated based on EDS–SEM results (Table 1).

In order to corroborate if the crystal size of the obtained phases was in the nanoscale, the powders were also investigated by TEM analyses. Fig. 3 shows typical bright field and dark field TEM images and the corresponding SAD pattern of the mechanically alloyed powders for 10 h. It can be noticed that crystal size of powders after 10 h of milling is below 20 nm.

3.2. Microstructural and structural characterization of bulk samples

Representative microstructure micrographs of the sintered sample are shown in Fig. 4. By SEM analyses (Fig. 4a), a characteristic microporous microstructure of mechanically alloyed and sintered materials is observed (4.18% of porosity). Two main phases, a continuous dark region and a discontinuous bright region, and submicron precipitates are detected. The grain size of the matrix and the precipitates formed during sintering was also identified by TEM observations. The Z-contrast TEM (STEM mode) image in Fig. 4b shows the presence of fine equiaxied precipitates with a width of several nanometers (<250 nm), which are homogeneously distributed within the complete matrix.

Through EDS/SEM mapping, the spatial distribution of elements in the formed phases of sintered sample was examined (Fig. 5). The bright phase has high Mo and Fe content, while the gray phase possesses high Al, Ni and Ti content. The Co is almost homogeneously distributed in both phases. Due to the precipitates size, the chemical composition of submicron precipitates (aluminum oxide) was

Table 1
Chemical composition of powders determined by EDS/SEM.

Sample	Milling time (h)	at.%					
		Al	Co	Fe	Mo	Ni	Ti
AlCoFeMoNiTi	0	*16.7	*16.7	*16.7	*16.7	*16.6	*16.6
	10	13.9	19.3	17.9	14.9	18.2	15.8

* Nominal composition.

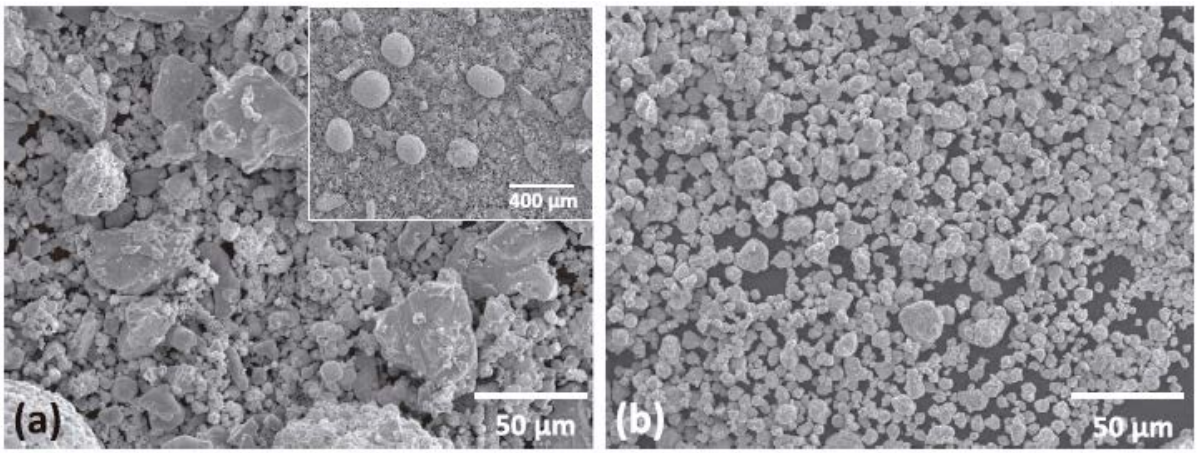

Fig. 2. SEM images of AlCoFeMoNiTi powders: (a) unmilled and (b) milled for 10 h.

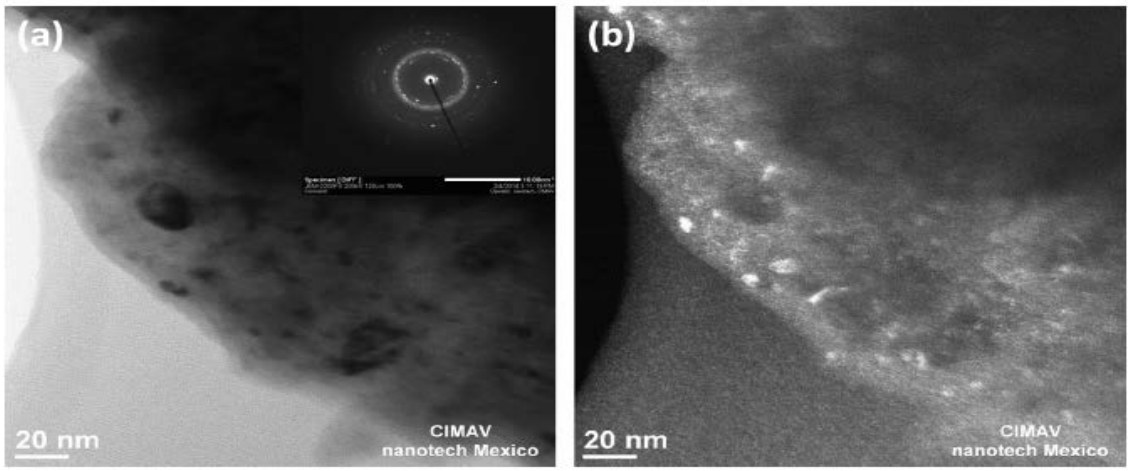

Fig. 3. TEM micrographs in (a) bright field and (b) dark field of as-milled powders after 10 h of milling.

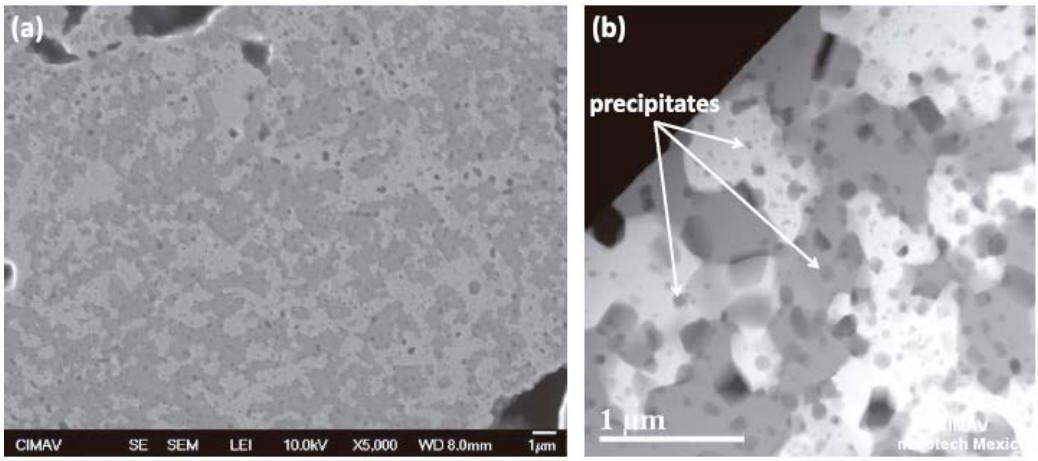

Fig. 4. Microstructure images of the sintered sample: (a) SE-SEM and (b) Z-contrast TEM (STEM mode).

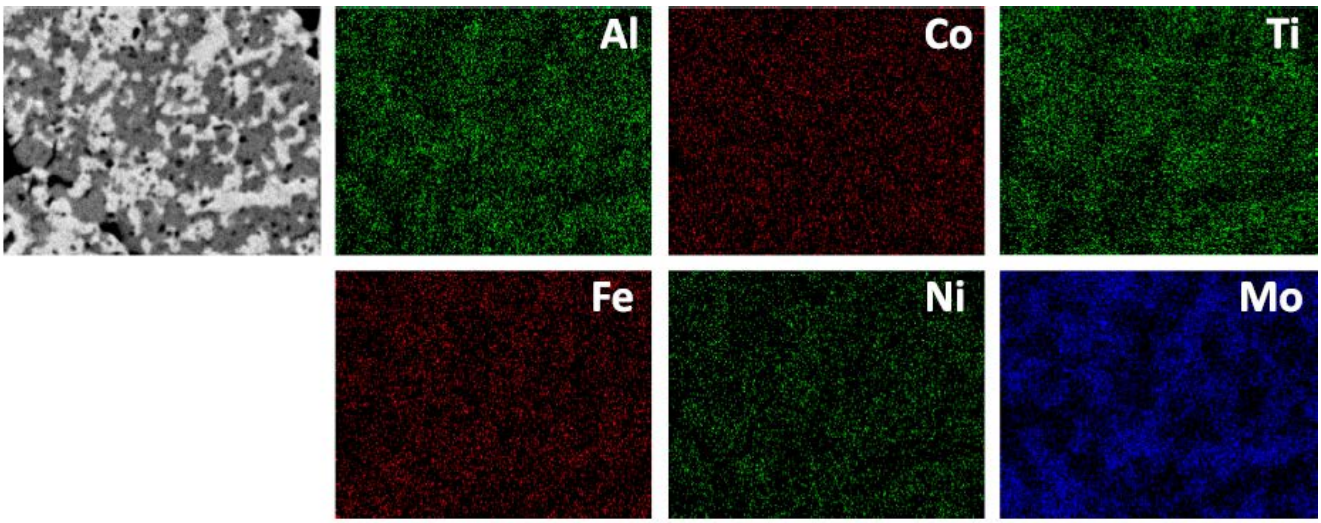

Fig. 5. SEM image of the sintered sample accompanying EDS-mapping.

Table 2
Chemical composition of individual phases of consolidated samples (EDS/TEM).

Sample	Phase	at.%						
		O	Al	Co	Fe	Mo	Ni	Ti
Sintered	Bright phase	–	1.6	18.4	28.9	37.6	7.9	5.6
	Gray phase	–	16.5	22.1	9.7	1.2	31.2	19.2
	Precipitates	16.2	37.3	9.2	10.6	13.8	7.3	5.5
As-cast	Continuous bright phase	–	1.9	17.9	32.6	30.7	8.1	8.8
	Discontinuous bright phase	–	2.3	1.7	4.7	86.0	0.5	4.9
	Gray phase	–	14.0	22.8	13.3	2.4	27.0	20.6
	Dark phase	16.5	–	–	–	1.9	–	81.6

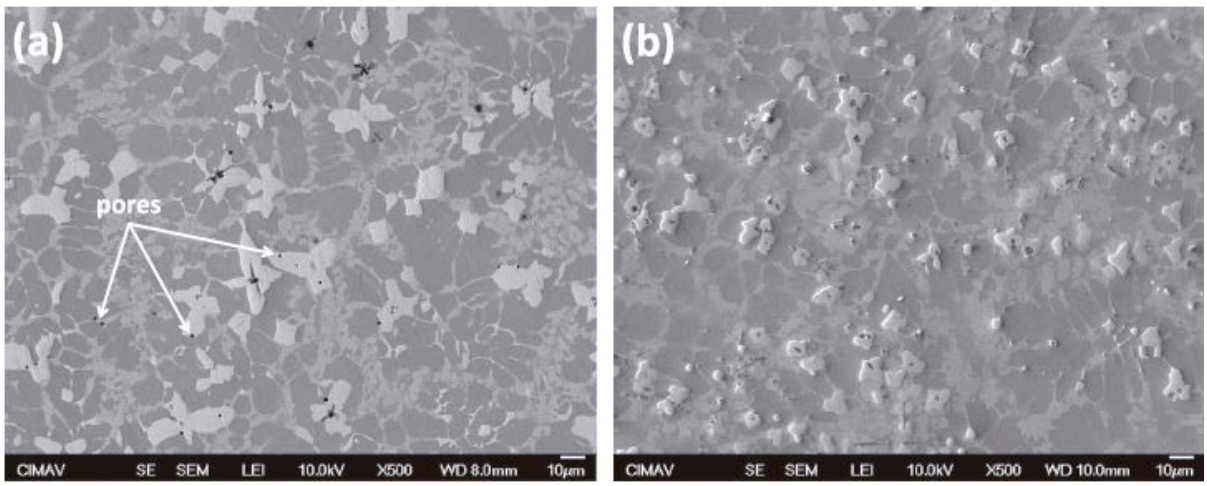

Fig. 6. SEM images of the as-cast samples: (a) un-milled and (b) milled powders.

examined by EDS/TEM microanalyses, the results are detailed further on in Table 2. As was expected, the processing route has a significant effect on the final microstructure of consolidated samples. Fig. 6 shows SEM images of representative microstructure after arc melting. In order to determine whether the effect of the mechanical alloying is kept after melting, the as-cast samples from un-milled (Fig. 6a) and milled powders (Fig. 6b) are shown. Both samples exhibit the formation of similar phases, a gray phase (Ni–Co–Ti-rich phase), a continuous bright phase (Fe–Mo–Co-rich phase), a discontinuous bright phase (Mo-rich phase) and a dark phase (Ti-rich phase). Contrary than expected by traditional metallurgy, the effect of mechanical alloying after melting is noticeable by a more uniform distribution of phases and their reduction in size.

In order to show in greater detail the microstructure after casting, in Fig. 7 are presented SEM (Fig. 7a) and Z-contrast TEM (STEM mode) image (Fig. 7b) of the as-cast sample from milled powders. The presence of Mo-rich and Ti-rich phases was determined by EDS/SEM mapping analysis (Fig. 7a). It is noticed that the synthesis process by arc melting leads to a considerable increase in the phases and

crystal size in comparison to the sintered sample. The formation of nano-scaled precipitates is not observed in the as-cast sample.

On the other hand, a low volume fraction of pores was observed in the as-cast samples. Before the consolidation processes (sintering and arc melting), the MA'ed powders were firstly cold pressed. During this process some air was entrapped between powder particles forming pores which were more reduced after melting, in

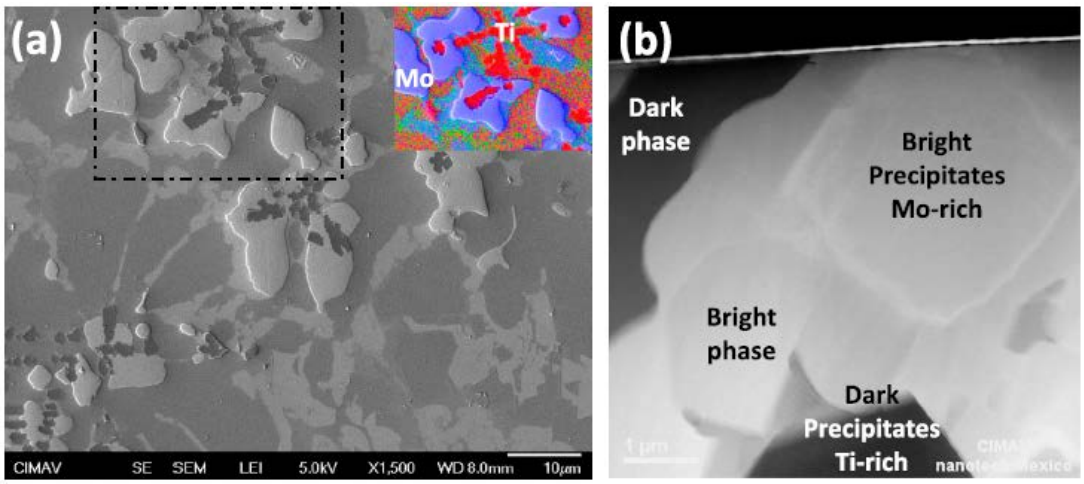

Fig. 7. Microstructure images of the as-cast sample: (a) SEM-LEI and EDS mapping and (b) Z-contrast TEM (STEM mode).

comparison to sintering process. The porosity for the as-cast sample from un-milled powders is 0.23%, while porosity of the as-cast sample from milled sample was not detected by optical and electron microscopy observations.

In Table 2 the semi-quantitative chemical composition of individual phases obtained by EDS/TEM analyses is presented. TEM observations were carried out on specimens with thickness lower than < 100 nm, making it possible to obtain semi-quantitative chemical composition of their phases with a minor error by EDS technique. The elements content in the main phases (gray and continuous bright

phases) are similar in both sintered and as-cast samples, in the other hand, only the sintered sample exhibit the formation of aluminum oxide precipitates. The major formation of pores in the sintered sample, due to the air trapped between powders during compaction, would also causes the oxidation of the more reactive elements, in this case the aluminum, as evidenced by the presence of oxygen and aluminum content in the observed precipitates (see Table 2). The sintered alloy possesses a greater chemical homogeneity, with an increase solid solubility, being that the as-cast sample exhibits segregation with the formation of two more phases a Mo-rich and a Ti-rich phases. In the Ti-rich phase oxygen content was also detected (~16 at.%), that suggests the formation of titanium oxide. These elements have greater atomic radius, and is possible that it causes a slower diffusion.

Since the development of high entropy alloys, it was proposed that phase formation involves the simultaneous movement of different atoms with different atomic radius, resulting in slow diffusion and hence the formation of nanophases [10]. In this work it is proposed that crystal refinement produced by the effect of MA remains after sintering due to the low diffusion effect during sintering at 1200 °C, in comparison with the diffusion of atoms during arc melting that reaches the liquid state.

Fig. 8 shows the XRD patterns of the consolidated samples. As observed in Fig. 8 by sintering the MA'ed powders, a mixture of different phases has been formed. A BCC Fe-type phase with a lattice parameter of 0.292 nm and a FCC phase with a lattice parameter of 0.414 nm are present. Besides, αCoMo and μCoMo-type phases (tetragonal structure) were identified according to the ICSD

102541 and 102544 cards, respectively, similar to the observed in a previous work that involved the characterization of a sintered NiCoAlFeMo alloy [11]. In the other hand, processing the MA'ed powders by arc melting results mainly in the formation of two BCC phases, BCC Fe-type (*a* = 0.294 nm) and BCC Mo-type (*a* = 0.314 nm), and a FCC phase with a lattice parameter similar to the FCC phase formed in the sintered sample (*a* = 0.415 nm). Additionally, a group of peaks were identified as Ti_2O, according

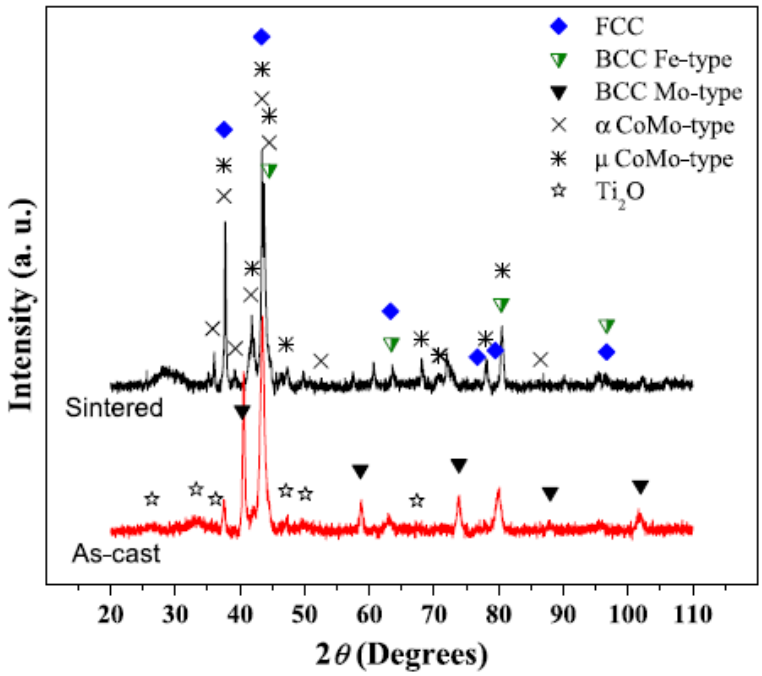

Fig. 8. XRD patterns of the bulk AlCoFeMoNiTi alloy in the (a) sintered and (b) as-cast conditions. BCC and FCC type phases are observed in both samples. Addition-ally small signals from Ti2O, aCoMo and lCoMo-type phases were detected.

to the ICDD 96–900-4140 card, was observed. It is suggested that the peaks identified as Mo-type and Ti_2O phases are related with the formation of microscale Mo-rich and Ti-rich phases present in the as-cast sample. The formation of Ti_2O is corroborated by the previous EDS/TEM results (see Table 2).

3.3. Microhardness

The high entropy alloys exhibit high hardness that varies widely according to the contents of the elements that compose them, but the processing route should also have a significant effect. Wang et al. [12] reported a hardness value of 500 HV for an AlCoCrFeNi alloy and Hsu et al. [13] reported a hardness of 730 HV for an AlCoCrFeNiMo0.5 system. Both alloys were produced by arc melting under a protective atmosphere of argon. It is evident that the addition of Mo has a significant effect on the hardness.

If the mechanical alloying is used for the synthesis of HEAs, the alloys can result in microcrystalline, sub-microcrystalline or even nanocrystalline alloys, so that their mechanical properties can be increased [14]; [15] ; [16]. In a previous study of our research group, nanocrystalline NiCoAlFeMo and NiCoAlFeTi systems were processed by mechanical alloying and subsequent conventional sintering

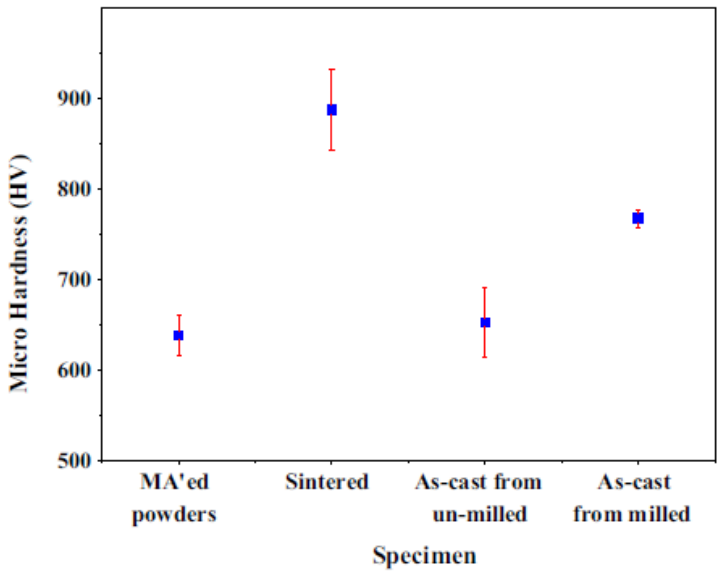

Fig. 9. Microhardness of milled powders and bulk samples.

process, they reached hardness of 896 and 807 HV, respectively. Hence, it was interesting to evaluate the microhardness of an equiatomic alloy combining the addition of Mo and Ti, and use to different processing routes.

The characteristic of the starting nanocrystalline MA'ed material in this work should have a significant effect on the final properties of the consolidated samples. However, as it was mentioned earlier, cold pressing of MA'ed powders caused the formation of pores in sintered samples.

Thus, it is expected that the mechanical properties of the sintered samples become worse in comparison to the as-cast sample. The studied arc melted and sintered specimens were examined by microhardness testing, which is one of the simple and easiest techniques to find the tendency of mechanical properties of the studied alloys regarding to the fabrication process. The results of microhardness test are shown in Fig. 9. The highest hardness values was achieved by the sintered sample (887 HV) followed by the as-cast sample from milled powder (767 HV) and as-cast sample from un-milled (652 HV). According to the hardness it can be corroborate that the effect of mechanical alloying in the enhance of mechanical performance is maintained after melting. A greater chemical homogeneity (less formed phases) in the sintered sample, its lower grain size after sintering in comparison to the as-cast sample, and the formation of nanocrystalline precipitates lead to the increase in microhardness, even with a greater porosity than the as-cast sample.

4. Conclusions

A nanocrystalline AlCoFeMoNiTi alloy was successful synthesized by mechanical alloying. Consolidated samples were obtained by two different routes, sintering and arc melting, presenting different microstructures respect to formed phases and grain size. According to electron microscopy observations, both alloys exhibit the formation of two main phases which are similar in chemical composition, a bright Fe–Mo–Co-rich phase and a gray Ni–Ti–Co-rich phase. The microstructural differences are as-cast sample also presents the formation of Mo-rich and Ti-rich phases, while aluminum oxide precipitates were only observed in the sintered sample. According to XRD results, both samples exhibit the formation of a BCC Fe-type and a FCC phases; sintered sample also exhibits the formation of tetragonal CoMo-type phases. The microhardness results showed that sintered sample reached the highest hardness. Even with the presence of a major porosity in the sintered specimen, the microhardness of this sample is around 15% higher than the as-cast sample from milled powders; in turn this is 17% higher than the as-cast sample from un-milled powders. The effect of mechanical alloying is maintained after arc melting as evidenced the increase of hardness.

Acknowledgements

FJBL was supported as a graduate student by CONACYT (grant 241960). This research was supported by CONACYT-Red Temática de Nanociencias y Nanotecnología (0124623) and Red Temática de Ciencia y Tecnología Espaciales (0170962 and 0170617). The technical assistance of K. Campos-Venegas, W. Antunez-Flores, O.O. Solis-Canto, C.E. Ornelas-Gutiérrez, E. Torres-Moye and J.E.

Ledezma-Sillas is greatly appreciated.

References

[1] J.W. Yeh, S.K. Chen, S.J. Lin, J.Y. Gan, T.S. Chin, T.T. Shun, et al., Adv. Eng. Mater. 6 (2004) 299–303.

[2] A. Gali, E.P. George, Intermetallics 39 (2013) 74–78.

[3] J.Y. He, W.H. Liu, H. Wang, Y. Wu, X.J. Liu, T.G. Nieh, et al., Acta Mater. 62 (2013) 105–113.

[4] W.H. Liu, Y. Wu, J.Y. He, T.G. Nieh, Z.P. Lu, Scripta Mater. 68 (2013) 526–529.

[5] F. Otto, A. Dlouhy´ , Ch. Somsen, H. Bei, G. Eggeler, E.P. George, Acta Mater. 61 (2013) 5743–5755.

[6] C.M. Liu, H.M. Wang, S.Q. Zhang, H.B. Tang, A.L. Zhang, J. Alloys Comp. 583 (2014) 162–169.

[7] Y.L. Chen, Y.H. Hu, C.W. Tsai, C.A. Hsieh, S.W. Kao, J.W. Yeh, T.S. Chin, S.K. Chen,

J. Alloys Comp. 477 (2009) 696–705.

[8] I. Kunce, M. Polanski, J. Bystrzycki, Int. J. Hydrogen Energy 39 (2014) 9904–9910.

[9] C.E. Lyman, D.E. Newbury, J.I. Goldstein, D.B. Williams, A.D. Roming Jr., J.T. Armstrong, P. Echlin, C.E. Fiori, D.C. Joy, E. Lifshin, K.R. Peters, Scanning Electron Microscopy, X-Ray Microanalysis and Analytical Electron Microscopy, Plenum Press, New York, 1990.

[10] J.W. Yeh, Y.L. Chen, S.J. Lin, S.K. Chen, Mater. Sci. Forum 560

(2007) 1–9.

[11] C.D. Gómez-Esparza, J. Camarillo-Cisneros, I. Estrada-Guel, J.G. Cabañas-Moreno, J.M. Herrera-Ramírez, R. Martínez-Sánchez, J. Alloys Comp. 615 (2014) S638–S644.

[12] W. Woei-Ren, W. Wei-Lin, W. Shang-Chih, T. Yi-Chia, L. Chun-Hui, Y. Jien-Wei, Intermetallics 26 (2012) 44–51.

[13] H. Chin-You, W. Woei-Ren, T. Wei-Yeh, C. Swe-Kai, Y. Jien-Wei, Adv. Eng. Mater. 12 (2010) 44–49.

[14] C. Li, J.C. Li, M. Zhao, Q. Jiang, J. Alloys Comp. 475 (2009) 752–757.

[15] S. Varalakshmi, M. Kamaraj, B.S. Murty, J. Alloys Comp. 460 (2008) 253–257.

[16] S. Varalakshmi, G. Appa Rao, M. Kamaraj, B.S. Murty, J. Mater. Sci. 45 (2010) 5158–5163.